Elimination of scattered gamma rays from injection sites using upper offset energy windows in sentinel lymph node scintigraphy

doi: 10.1097/MNM.0000000000000281

Original Article

Elimination of scattered gamma rays from injection sites using upper offset- energy windows in sentinel lymph node scintigraphy

Hiroto Yoneyama[1], Hiroyuki Tsushima[2], Masahisa Onoguchi[3],
Takahiro Konishi[1], Kenichi Nakajima[4], Seigo Kinuya[4]

[1] Department of Radiological Technology, Kanazawa University Hospital
[2] Department of Radiological Sciences, Ibaraki Prefectural University of Health Sciences
[3] Department of Health Science, Graduate School of Medical Science, Kanazawa University
[4] Department of Biotracer Medicine, Graduate School of Medical Science, Kanazawa University

For correspondence and reprints contact:
Hiroto Yoneyama
Department of Radiological Technology, Kanazawa University Hospital, 13-1 Takara-machi, Kanazawa 920-8641, Japan
Tel: 81-76-265-2000
Fax: 81-76-234-4311
E-mail address: kizu @cf6.so-net.ne.jp

Short running head: Elimination of scattered gamma rays

Authors must state all possible conflicts of interest in the manuscript, including financial, consultant, institutional and other relationships that might lead to bias or a conflict of interest. If there is no conflict of interest, this should also be explicitly stated as none declared. All sources of funding should be acknowledged in the manuscript. All relevant conflicts of interest and sources of funding should be included on the title page of the manuscript with the heading "Conflicts of Interest and Source of Funding"

Abstract

Objective: The identification of sentinel lymph nodes (SLNs) near injection sites is difficult, due to scattered gamma rays. The purpose of this study was to investigate the optimal energy windows for elimination of scattered gamma rays, to improve the detection of SLNs.

Methods: The clinical study group consisted of 56 female patients with breast cancer. While the energy was centred at 140 keV with a 20% window for Tc-99m, this energy window was divided into 5 sub-windows with every 4% in planar imaging. Regions of interest were placed on SLNs and background (BG), and contrast was calculated via a standard equation. The confidence levels of interpretations were evaluated using a 5-grade scale.

Results: The contrast provided by 145.6 keV ± 2% was the best, followed by 140 keV ± 2%, 151.2 keV ± 2%, 134.4 keV ± 2%, and 128.8 keV ± 2% in that order. When 128.8 keV ± 2% and 134.4 keV ± 2% were eliminated from 140 keV ± 10% (145.6 keV ± 6%), the contrast of SLNs improved significantly. The confidence levels of interpretation and detection rate provided by the planar images with 140 keV ± 10% were 4.74 ± 0.58 and

94.8% respectively, and those provided by 145.6 keV ± 6% were 4.94 ± 0.20 and 100%.

Conclusions: Because lower energy windows contain many scattered gamma rays, upper offset energy windows which exclude the lower energy windows improve the image contrast of SLNs near injection sites.

Keywords: Sentinel lymph node, Energy window, Planar images,

Scattered gamma rays, Breast cancer

Introduction

A sentinel lymph node (SLN) is defined as the lymph node that is first to receive lymphatic drainage from a tumour. When the SLN is tumor free, the nodal basin can be regarded as free of disease, and unnecessary dissection can be avoided [1]. Arm problems, such as numbness, pain, restricted arm mobility and lymphedema are influenced by the number of lymph nodes removed. Complications from axillary lymph node dissection may be reduced by limiting the extent of dissection using SLN biopsy [2, 3]. Preoperative detection of SLNs permits surgeons to locate nodes efficiently with a gamma probe during surgery, and lymphoscintigraphy can accurately reveal the localisations of SLNs in this context [4, 5]. One of the major problems in lymphoscintigraphy is the inclusion of scattered gamma rays within the photo-peak energy window. In Compton scattering, the energy of scattered gamma rays depends on the scatter angle (Fig. 1) [6]. Scattered gamma rays sometimes hamper the identification of SLNs near injection sites. Therefore, we hypothesised that optimal energy windows may eliminate scattered gamma rays, which could result in improved SLN detection. The purpose of this study was to investigate the optimal energy windows for elimination of scattered gamma rays, and the method was applied to clinical studies.

Methods

Phantom study

To evaluate the optimal energy window and the difference in collimator characteristics, the low-energy high-resolution (LEHR) collimator and the low-to medium-energy general-purpose (LMEGP) collimator, for SLN lymphoscintigraphy in breast cancer patients, we used both injection site phantoms and lymph node phantoms, to simulate injection sites and SLNs. Injection site phantoms were 2 cm in diameter and 1 cm thick, and contained 40 MBq (1.1 mCi) of Tc-99m pertechnetate. Lymph node phantoms were 5 or 10 mm in diameter and 1 cm thick, and contained 1.6, 4.0, 25.0, and 400.0 kBq (0.04, 0.11, 0.68, or 10.80 kCi) of Tc-99m pertechnetate. A total of 8 lymph node phantoms were aligned 3 and 6 cm from the centre of the injection site phantom, in both the horizontal direction and oblique direction. The energy was centred at 140, 143, 146, 149 and 152 keV, with a 15% window. Regions of interest were placed on SLNs and background (BG), and contrast was calculated with the following equation: Contrast = (SLN activity - BG activity) / (SLN activity + BG activity).

Clinical study

The study sample consisted of 56 consecutive female patients aged 56.1 ± 13.1 years, with breast cancer that was histologically diagnosed between November

2013 and July 2014 inclusively. One patient was excluded because written informed consent was not obtained. The tumour was on the right side in 22 patients and the left side in 32, and was bilateral in 2 patients. A 37 MBq dose of Tc-99m phytate (Fujifilm RI Pharma, Japan) was injected subcutaneously around the tumour. Location markers containing 0.3 MBq (8.1μCi) of Tc-99m pertechnetate were placed at the centre of the sternal notch and the xiphoid process. Planar imaging was performed at 10 min and 3 - 4 hours after injection. The injection sites were not covered with a lead shield. The counts in the planar image were collected for 6 min in a 256 × 256 matrix, with a low-to medium-energy general-purpose (LMEGP) collimator. While the energy was centred at 140keV with a 20% window for Tc-99m, this energy window was divided into 5 sub-windows with every 4% in planar imaging. The energy window was centred at 128.8 keV ± 2%, 134.4 keV ± 2%, 140 keV ± 2%, 145.6 keV ± 2% and 151.2keV ± 2% without overlaps. A dual-head gamma camera equipped with a LMEGP collimator (Symbia T6; Siemens, Erlangen, Germany) was used for planar imaging. When the SLNs were not identified clearly, such as when the tumour was located in the upper lateral region, additional directional views were acquired. Five nuclear medicine physicians evaluated the planar images, and recorded their degrees of confidence in interpreting images with regard to the presence or absence of SLNs. The confidence

levels of interpretation were evaluated using a 5-grade scale: 1, definitely not identified; 2, probably not identified; 3, equivocal; 4, probably identified; and 5, definitely identified. Detection rate was calculated as the number of patients whose average confidence levels of interpretation were more than 4, divided by the total number of patients. When the average confidence levels of interpretation were more than 4.6, the clinical interpretation was that the SLN had been definitely identified, and when it was less than 2.9 it was that it had not been identified. Average scores between 3.0 and 3.9 were deemed equivocal, and scores between 4.0 and 4.5 were deemed to indicate that the SLN was probably identified. Confidence levels of interpretation were expressed as mean ± standard deviation (SD) and median. The confidence levels were compared using the Wilcoxon signed-rank test. Regions of interest were placed on SLNs and BG, and contrast was calculated with the following equation: Contrast = (SLN activity - BG activity) / (SLN activity + BG activity). Contrast and SLN counts were compared using the Student's t-test. Statistical significance was defined as $p < 0.05$. The study protocol was approved by the ethical committee of Kanazawa university hospital, and written informed consent was obtained from all patients.

Results

Phantom study

Images derived from the phantom study are shown in Fig. 2. Lymph node and injection site phantom images were obtained with the LMEGP collimator (a - c) and the LEHR collimator (d, e). Lymph node phantoms contained 1.6, 4.0, 25.0, and 400.0 kBq (0.04, 0.11, 0.68, and 10.80 μCi) of Tc-99m pertechnetate. Contrast was greatly affected by the radioactivity in the lymph nodes, and the distance from the injection site to the lymph nodes. Upper offset- energy windows showed better separation of SLNs from the injection site. Compared with the same radioactivity in lymph nodes and the same distance from the injection sites to the lymph nodes, image contrast was improved by using upper off-set energy windows (Table 1). Star-shaped artifacts radiating from the injection-site phantom occurred by using the LEHR collimator. Star-shaped artifacts were reduced using the LMEGP collimator.

Clinical study

The confidence level of interpretation and the detection rate provided by the planar images with 140 keV ± 10% were 4.74 ± 0.58 and 94.6% respectively. Average SLN counts and background for every 4% energy window are shown in Fig. 3. Lower energy windows contained many scattered gamma rays. The contrast provided by 145.6 keV ± 2% was the best (0.743 ± 0.20), followed by 140 keV ± 2% (0.734 ± 0.20), 151.2

keV ± 2% (0.634 ± 0.26), 134.4 keV ± 2% (0.630 ± 0.23), and 128.8 keV ± 2% (0.409 ± 0.24) (Fig. 4). The contrast provided by 140 keV ± 10% was 0.635 ± 0.22. The planar images generated with energy windows centred at 128.8 keV ± 2%, 134.4 keV ± 2%, 140 keV ± 2%, 145.6 keV ± 2% and 151.2 keV ± 2% are shown in Fig. 5. When 128.8 keV ± 2% and 134.4 keV ± 2% were eliminated from 140 keV ± 10% (145.6 keV ± 6%), the SLN contrast improved significantly, from 0.635 ± 0.22 to 0.730 ± 0.20 ($p = 0.0063$) and SLN counts decrease by approximately 42% compared with 140 keV ± 10% (Fig. 6). Even when the 128.8 keV ± 2% count was eliminated from the 140 keV ± 10% count (142.8 keV ± 8%), the improvement in SLN contrast (from 0.635 ± 0.22 to 0.692 ± 0.21) was not significant, and SLN counts were reduced by approximately 13% compared with 140 keV ± 10% (Fig. 7). The confidence levels of interpretation and detection rate provided by the planar images with 145.6 keV ± 6% were 4.94 ± 0.20 and 100% respectively. There was a significant difference between the confidence levels of interpretations associated with 140 keV ± 10% and 145.6 keV ± 6% ($p < 0.0001$). Relationships between SLN contrast and clinical interpretation, and between SLN counts and clinical interpretation are shown in Fig. 8. Clinical interpretations of SLNs tended to be significantly influenced by image contrast, rather than SLNs counts.

Discussion

Lymphoscintigraphy is a useful test for confirming the locations of SLNs preoperatively, making the biopsy of SLNs less invasive and ensuring that SLNs in unexpected locations are not missed. SLNs often appear only very faintly, because the radioactivity that flows into them is only a small proportion of the injected dose [7]. Due to the poor energy resolution of the NaI(Tl) scintillation crystal used in the imaging system (approximately 10% full width at half maximum, 140 keV) [8], the detection of some scattered gamma rays in the conventional photo-peak energy window is unavoidable. The reduced image quality is mainly due to Compton-scattered gamma rays contained in the preset energy window. Several techniques have been proposed for Compton scatter compensation [9-11].

Glass et al. [12] reported that adjustment of the energy window may improve the imaging of SLNs located close to injection sites. By acquiring only the high-energy component of the photo-peak, scattered gamma rays are reduced. Krynyckyi et al. [13] have shown that when the centre of the energy window was shifted upward by 5 keV, improved images with less background were obtained. Tsushima et al. [14, 15] reported that the contrast and detection capacity of lymphoscintigraphy were improved by using medium-energy collimator and an upper offset energy window of 146 keV ± 5%.

Since lower energy windows contain a significant amount of scattered gamma rays, the image contrast was reduced when including the lower energy windows, especially near injection sites. The detectability of SLNs was more affected by image contrast than SLN counts, when the SLNs were located close to injection sites. Although a few studies have investigated optimal energy windows for SLN imaging, none have compared conventional energy windows with optimal energy windows in a clinical setting. In our study, when an upper offset energy window, such as 145.6 keV ± 6% (after subwindows of 128.8 keV ± 2% and 134.4 keV ± 2% were eliminated from 140 keV ± 10%) was used for lymphoscintigraphy, the contrast was significantly improved. Although the SLN counts using 145.6 keV ± 6% were lower than those with 140 keV ± 10%, upper offset energy windows yield better separation of SLNs from injection sites. However, aspect of the counts, and the contrast of the SLNs meant that the improvement was a trade-off issue. When the 5 offset energy windows without overlaps were used, we could adjust optimal energy windows depending on the situation after imaging. When SLNs are near the injection sites, planar images should be acquired with 145.6 keV ± 6%. We found that an image contrast of 0.5 and SLN count of 100 yielded a suitable threshold level for interpretation of ‘definitely identified’ SLNs. A contrast value of 0.5 indicates that the SLN counts are 3 times greater than the

background counts.

The information from lower energy windows may rule out artifact derived from injection sites. Although the photo-peak of Tc-99m occurred at approximately 141 keV, scattered gamma rays might shift the peak to the lower energy side. The energy of Compton-scattered gamma rays is reduced, depending on their scattering angle. Our 5 energy windows-based method could distinguish SLNs, and eventually reduced scattered gamma rays in planar images. When we eliminated some fractions of the lower energy windows, scattered gamma rays could be reduced while maintaining the primary gamma rays.

Some studies have discussed the optimal collimator choice for planar imaging [15-19]. In most cases, SLNs that were not detected were located near injection sites. Collimator imaging with lower septal penetration is effective for the accurate identification of SLNs close to injection sites; lower septal penetration, such as LMEGP collimator, reduces the appearance of star-shaped artifacts from injection sites.

The main variable parameter of the radio-pharmaceuticals used for SLN detection is particle size [4]. Phytate labelled with Tc-99m, which is mainly used for SLNs scintigraphy in Japan, forms a colloid in vivo upon reacting with ionised calcium. Tavares et al. [20] reported that a high rate (98%) of SLNs detection was achieved with

a gamma probe and SLN scintigraphy using Tc-99m phytate. In addition, if SLNs are not clearly detected in the initial planar imaging, massaging of stagnate injection sites is useful to enhance regional tracer flow. Multi-direction views are also helpful to detect SLNs when the tumours are located near axillary nodes that may be concealed behind injected radioactivity [21].

Conclusion

Because lower energy windows contain many scattered gamma rays, upper offset energy windows which exclude lower energy windows improve the image contrast of SLNs near injection sites. In our phantom and clinical studies investigating optimal energy windows, 145.6 keV ± 6% was appropriate for SLN scintigraphy near injection sites. When the 5 offset energy windows without overlaps were used, we could derive an optimal energy window appropriate for the situation after imaging.

Acknowledgments

This work was supported by Grants-in-Aid for Scientific Research in Japan (No. 26931049). The authors thank Shinro Matsuo, Daiki Kayano, Hiroshi Wakabayashi, Anri Inaki and all nuclear medicine physicians at the Kanazawa

University Hospital, for their lymphoscintigraphy interpretations. We gratefully thank M. Tobisaka, M. Kawamura, K. Noto, and all radiological technologists at the Kanazawa University Hospital for providing technical support.

References

1. Morton DL and Chan AD The concept of sentinel node localization: How it started. *Semin Nucl Med* 2000:4-10.
2. Schrenk P, Rieger R, Shamiyeh A and Wayand W Morbidity following sentinel lymph node biopsy versus axillary lymph node dissection for patients with breast carcinoma. *Cancer* 2000;**88**:608-614.
3. Veronesi U, Paganelli G, Viale G, Luini A, Zurrida S, Galimberti V*, et al.* A randomized comparison of sentinel-node biopsy with routine axillary dissection in breast cancer. *N Engl J Med* 2003;**349**:546-553.
4. Alazraki NP, Styblo T, Grant SE, Cohen C, Larsen T and Aarsvold JN Sentinel node staging of early breast cancer using lymphoscintigraphy and the intraoperative gamma-detecting probe. *Semin Nucl Med* 2000:56-64.
5. Moncayo VM, Aarsvold JN, Grant SF, Bartley SC and Alazraki NP Status of sentinel lymph node for breast cancer. *Semin Nucl Med* 2013;**43**:281-293.
6. Japan Radioisotope Association. Radioisotope Pocket Data Book (11th Edition) 2011
7. Fujii H, Kitagawa Y, Kitajima M and Kubo A Sentinel nodes of malignancies originating in the alimentary tract. *Ann Nucl Med* 2004;**18**:1-12.
8. Kwo D, Barber H, Barrett H, Hickemell T and Woolfenden J Comparison of NaI(T1), CdTe, and HgI2 surgical probes: effect of scatter compensation on probe performance. *Med Phys* 1991;**18**:382-389.
9. de Nijs R, Lagerburg V, Klausen TL and Holm S Improving quantitative dosimetry in (177)Lu-DOTATATE SPECT by energy window-based scatter corrections. *Nucl Med Commun* 2014;**35**:522-533.
10. Noori-Asl M, Sadremomtaz A and Bitarafan-Rajabi A Evaluation of three scatter correction methods based on estimation of photopeak scatter spectrum in SPECT imaging: A simulation study. *Phys Med* 2014.
11. Ichihara T, Ogawa K, Motomura N, Kubo A and Hashimoto S Compton Scatter Compensation Using the Triple-Energy Window Method for Single-and Dual-isotope SPECT *J Nucl Med* 1993;**34**:2216-2221.
12. Glass EC, Essner R and Giuliano AE Sentinel node localization in breast cancer. *Semin Nucl Med* 1999:57-68.
13. Krynyckyi BR, Miner M, Ragonese JM, Firestone M, Kim CK and Machac J Technical aspects of performing lymphoscintigraphy optimization of methods used to obtain images. *Clin Nucl Med* 2000;**25**:978-985.
14. Tsushima H, Takayama T, Kizu H, Yamanaga T, Shimonishi Y, Kosakai K*, et al.*

Advantages of upright position imaging with medium-energy collimator for sentinel node lymphoscintigraphy in breast cancer patients. *Ann Nucl Med* 2007;**21**:123-128.

15. Tsushima H, Takayama T, Yamanaga T, Kizu H, Shimonishi Y, Kosakai K*, et al.* Usefulness of medium-energy collimator for sentinel node lymphoscintigraphy. *J Nucl Med Technol* 2006;**34**:153-159.
16. Lemstra C, Broersma M, Poot L and Jager PL Sentinel node detection in patients with breast cancer low-energy all-purpose collimator or medium-energy collimator? *Clin Nucl Med* 2004;**29**:609-613.
17. Yoneyama H, Tsushima H, Kobayashi M, Onoguchi M, Nakajima K and Kinuya S Improved detection of sentinel lymph nodes in SPECT/CT images acquired using a low-to medium-energy general-purpose collimator. *Clin Nucl Med* 2014;**39**:e1-6.
18. Aryana K, Gholizadeh M, Momennezhad M, Naji M, Aliakbarian M, Forghani MN*, et al.* Efficacy of high-energy collimator for sentinel node lymphoscintigraphy of early breast cancer patients. *Radiol Oncol* 2012;**46**:75-80.
19. Kobayashi M, Wakabayashi H, Kayano D, Konishi T, Kojima H, Yoneyama H*, et al.* Application of a medium-energy collimator for I-131 imaging after ablation treatment of differentiated thyroid cancer. *Ann Nucl Med* 2014;**28**:551-558.
20. Tavares MG, Sapienza MT, Galeb NA, Belfort FA, Costa RR, Osório CA*, et al.* The use of 99mTc-phytate for sentinel node mapping in melanoma, breast cancer and vulvar cancer: a study of 100 cases. *Eur J Nucl Med* 2001;**28**:1597-1604.
21. Koizumi M, Nomura E, Yamada Y, Takiguchi T, Ishii M, Yamashita T*, et al.* Improved detection of axillary hot nodes in lymphoscintigraphy in breast cancer located in the upper lateral quadrant with additional projection imaging. *Ann Nucl Med* 2004;**18**:707-710.

Legends for illustrations

Table 1. Image contrast and counts from lymph node phantoms. The energy windows were centered 140 keV, 143 keV, 146 keV, 149 keV and 151 keV ± 7.5%. Lymph node phantoms contained 1.6 (1st row), 4.0 (2nd row), 25.0 (3rd row), and 400.0 kBq (4th row) of Tc-99m pertatechnetate.

Fig. 1. Relationship between the energy of scattered gamma rays and their scatter angle, in Compton scattering.

Fig. 2. Comparison of lymph nodes and injection site phantom images obtained with the low-to-medium-energy general purpose (LMEGP) collimator (a - c) and the low-energy high-resolution (LEHR) collimator (d, e). The energy windows were centred at 140 keV (a, d), 146 keV (b, e) and 151 keV (c) ± 7.5%. Lymph-node phantoms contained 1.6 (1st row), 4.0 (2nd row), 25.0 (3rd row), and 400.0 kBq (4th row) (0.04, 0.11, 0.68, and 10.80 μCi) of Tc-99m pertechnetate. Injection site phantoms contained 40 MBq (1.1 mCi) of Tc-99m pertechnetate. These images were displayed different maximum scale, normalized to lymph-node phantoms counts.

Fig. 3. The average SLN counts and background in planar images.

Fig. 4. Average SLN contrast obtained with 128.8 keV ± 2%, 134.4 keV ± 2%, 140 keV ± 2%, 145.6keV ± 2% and 151.2 keV ± 2%.

Fig. 5. Planar images of a 79-year-old female patient with breast cancer. Energy windows were centred at 128.8 keV ± 2% (a), 134.4 keV ± 2% (b), 140 keV ± 2% (c), 145.6 keV ± 2% (d), 151.2 keV ± 2% (e), 140 keV ± 10% (f) and 145.6 keV ± 6% (g).

Fig. 6. Planar images of a 67-year-old female patient with breast cancer. Energy windows were centred at 140 keV ± 10% (a) and 145.6 keV ± 6% (b).

Fig. 7. Average contrast of SLNs obtained with 140 keV ± 10%, 145.6 keV ± 6% and 142.8 keV ± 8%.

Fig. 8. Relationship between SLN contrast and clinical interpretation (a). Relationship between SLN counts and clinical interpretation (b).

Table 1　Image contrast (counts) of lymph node phantoms

Radioactivity of lymph node phantom (kBq)	Distance from the injection site phantom to the lymph node phantom									
	3 cm					6 cm				
	The center of energy windows (±7.5%)									
	140keV	143keV	146keV	149keV	151keV	140keV	143keV	146keV	149keV	151keV
1.6	n.d.	n.d.	n.d.	n.d.	n.d.	0.39 (52)	0.55 (36)	0.58 (30)	0.61 (25)	0.53 (21)
4.0	n.d.	n.d.	n.d.	n.d.	n.d.	0.62 (103)	0.80 (81)	0.83 (75)	0.79 (55)	0.75 (36)
25.0	0.21 (1122)	0.33 (1045)	0.47 (784)	0.59 (501)	0.64 (302)	0.91 (548)	0.94 (519)	0.95 (426)	0.95 (329)	0.94 (239)
400.0	0.87 (8816)	0.92 (8389)	0.95 (7353)	0.97 (5615)	0.98 (8002)	0.99 (7935)	0.99 (6976)	0.99 (5456)	0.99 (3684)	0.99 (3428)

n.d.: not detected

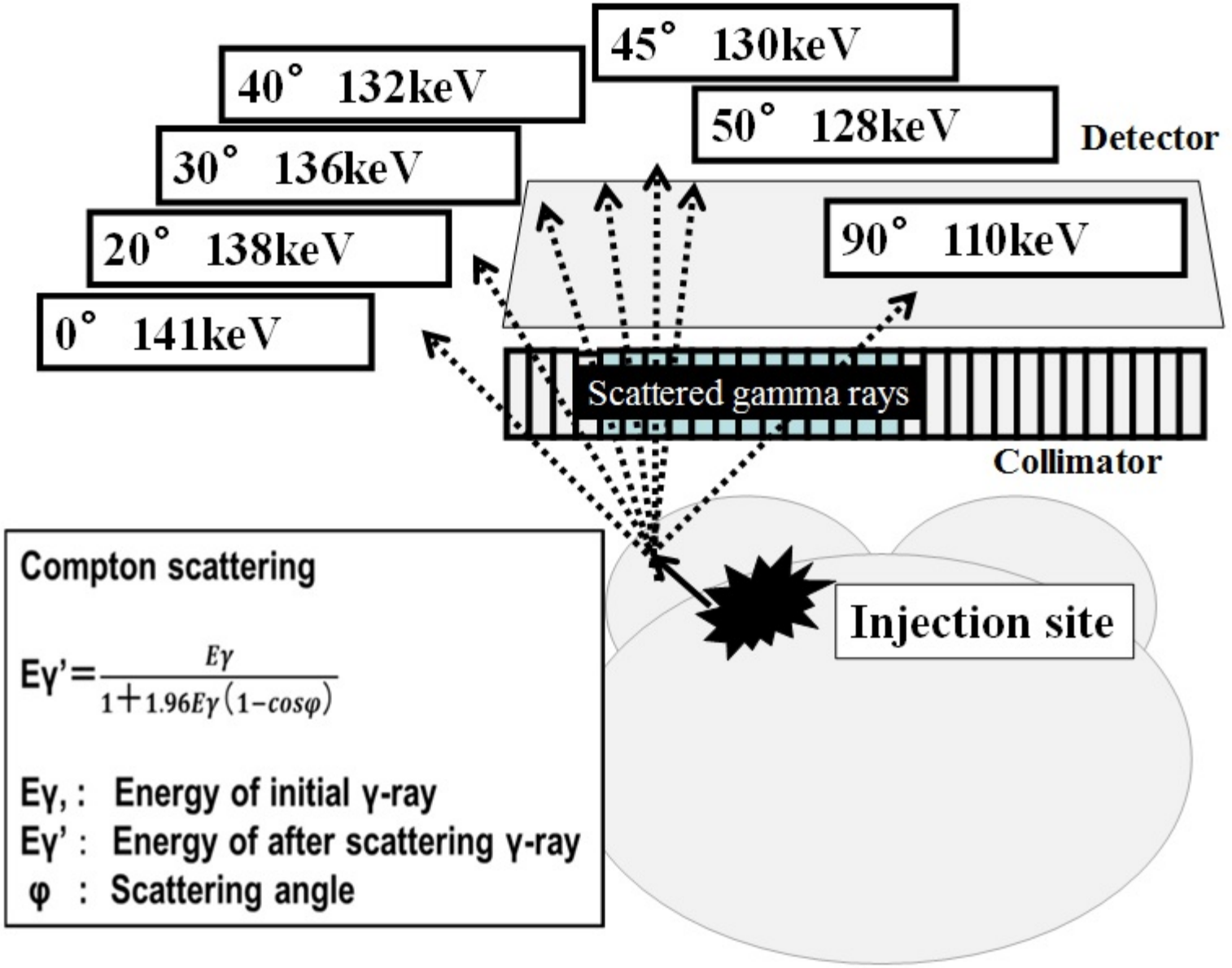
45° 130keV
40° 132keV
50° 128keV
Detector
30° 136keV
90° 110keV
20° 138keV
0° 141keV
Scattered gamma rays
Collimator
Injection site
Compton scattering
$E\gamma' = \frac{E\gamma}{1 + 1.96E\gamma(1 - cos\varphi)}$
Eγ, : Energy of initial γ-ray
Eγ' : Energy of after scattering γ-ray
φ : Scattering angle

Fig.1

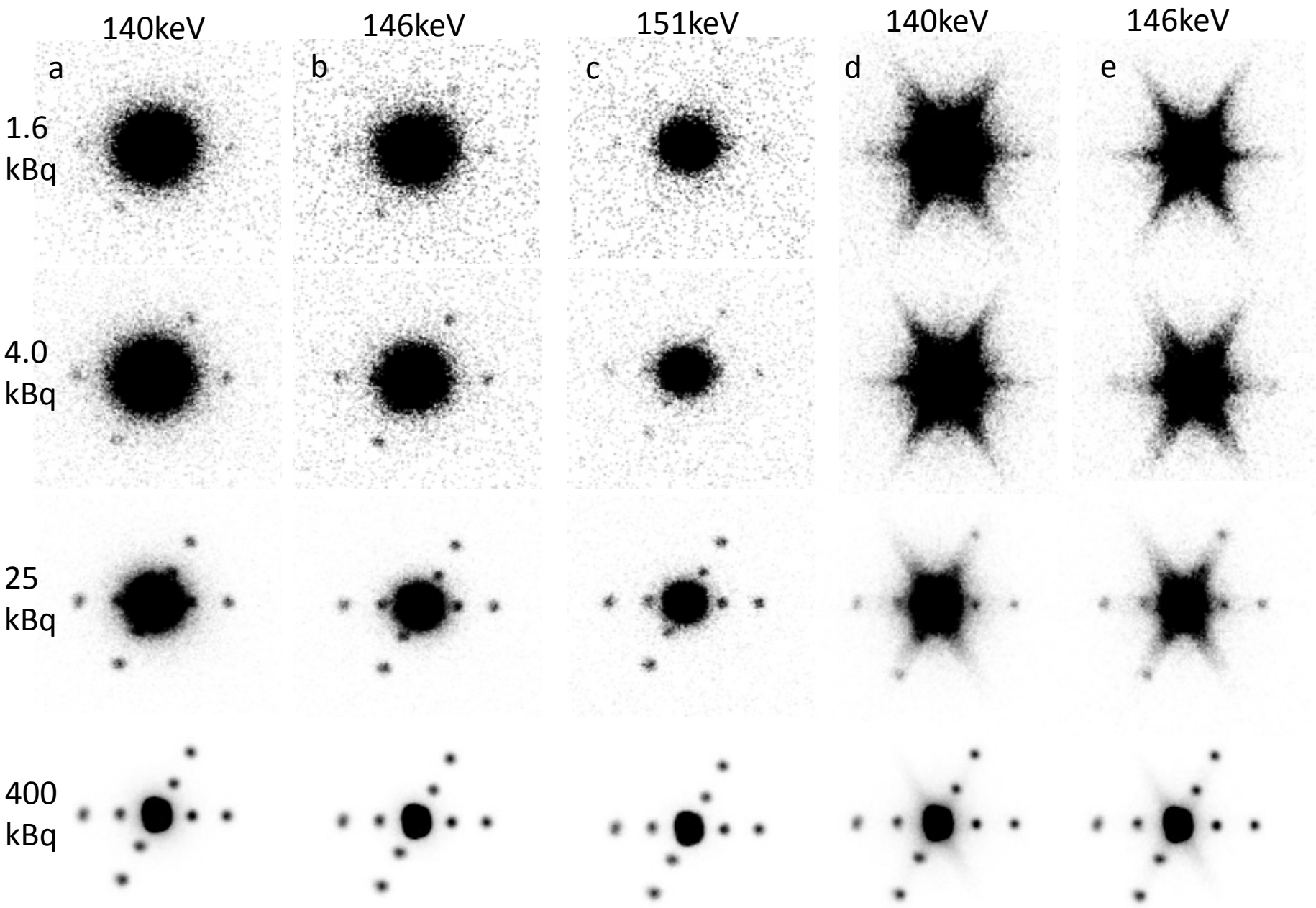
140keV
146keV
151keV
140keV
146keV
a
b
c
d
e
1.6 kBq
4.0 kBq
25 kBq
400 kBq

Fig.2

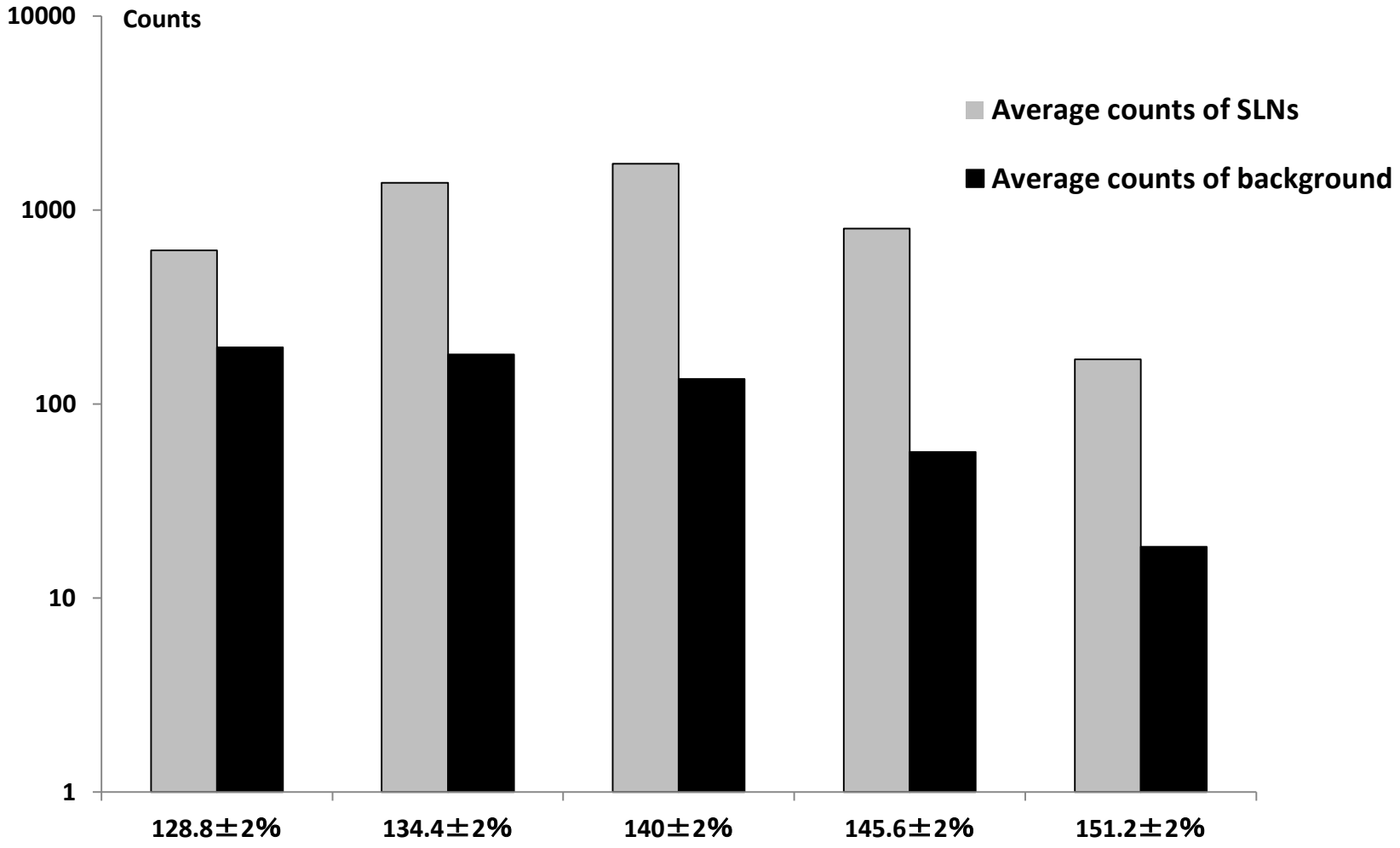
10000
Counts
1000
100
10
1
Average counts of SLNs
Average counts of background
128.8±2%
134.4±2%
140±2%
145.6±2%
151.2±2%

Fig.3

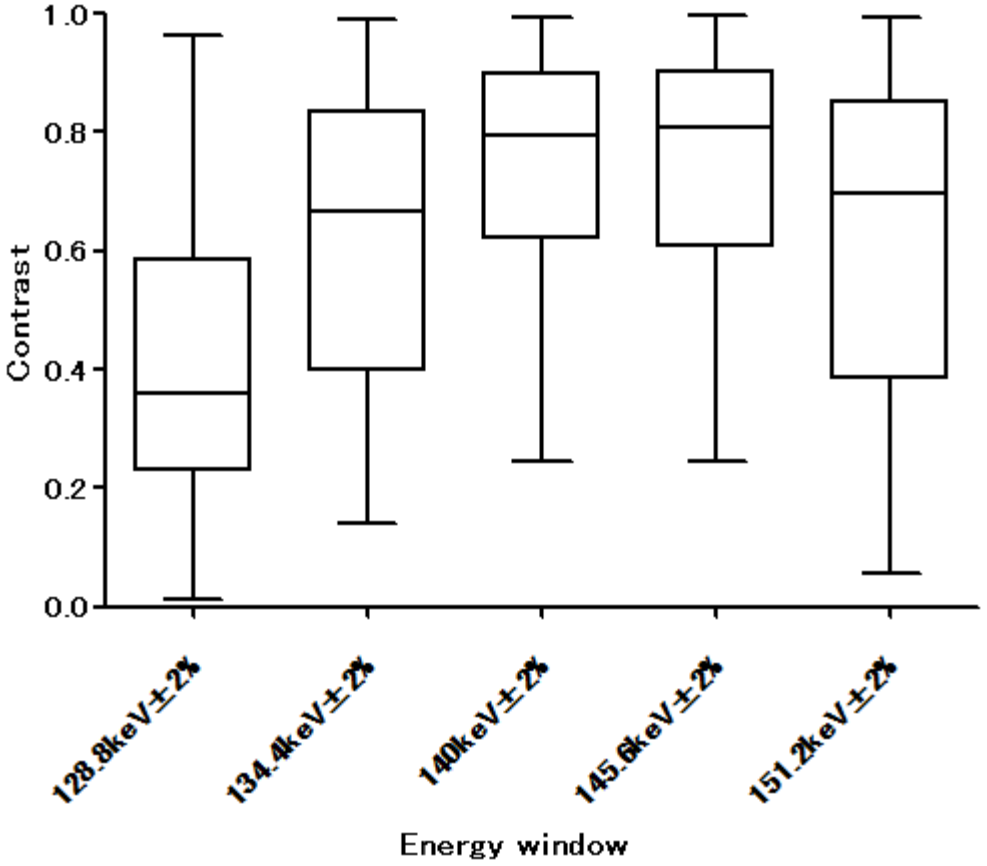
1.0
0.8
0.6
0.4
0.2
0.0
Contrast
128.8keV±2%
134.4keV±2%
140keV±2%
145.6keV±2%
151.2keV±2%
Energy window

Fig.4

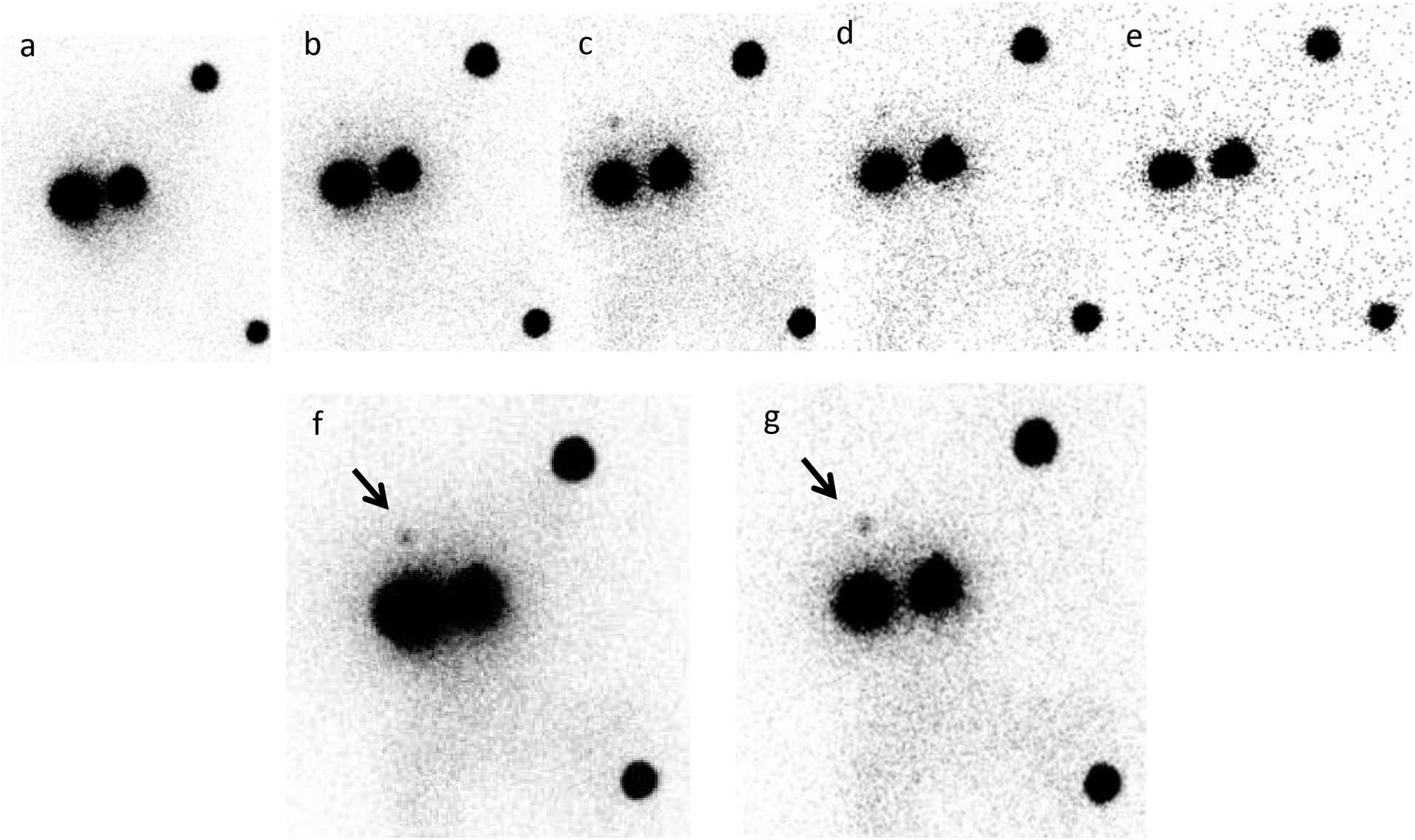

Fig.5

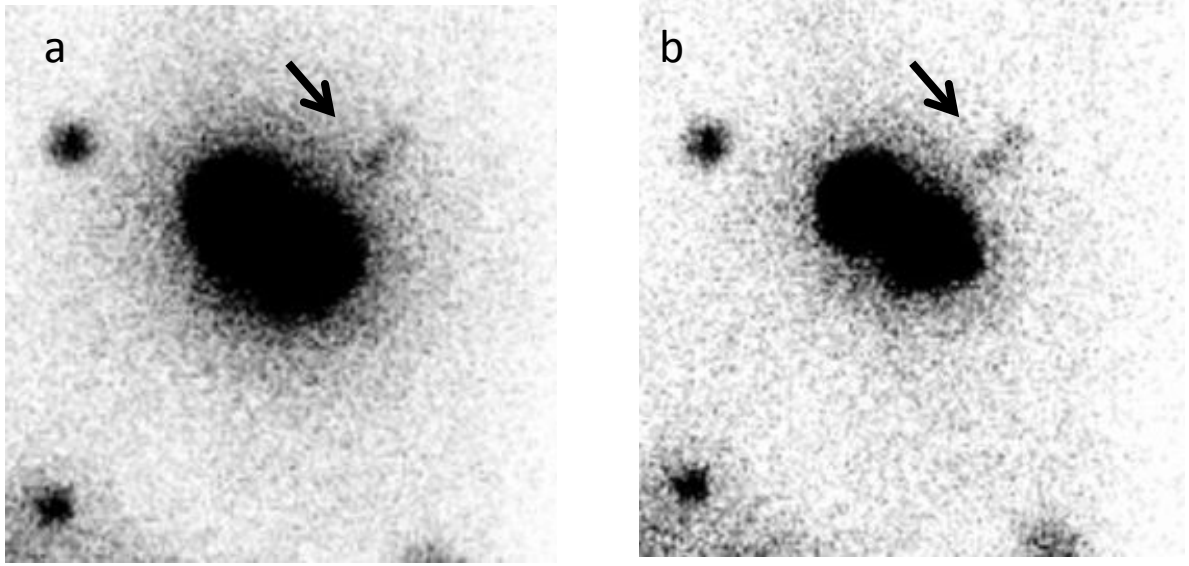

Fig.6

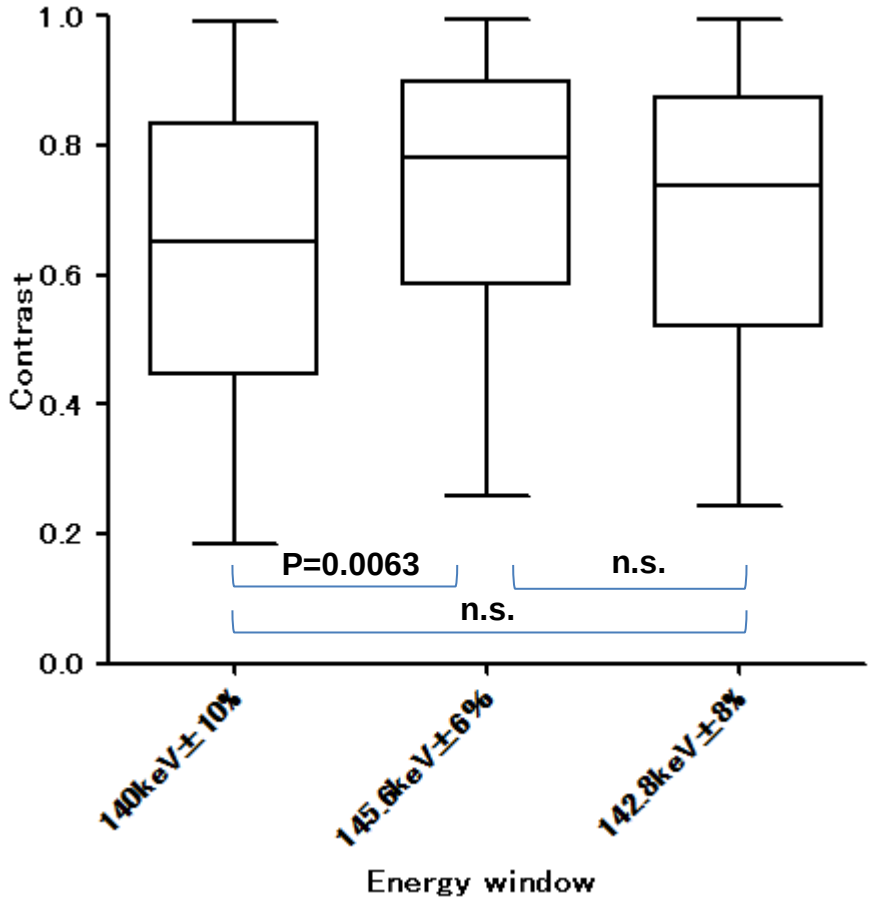
1.0
0.8
0.6
0.4
0.2
0.0
Contrast
P=0.0063
n.s.
n.s.
140keV±10%
145.6keV±6%
142.8keV±8%
Energy window

Fig.7

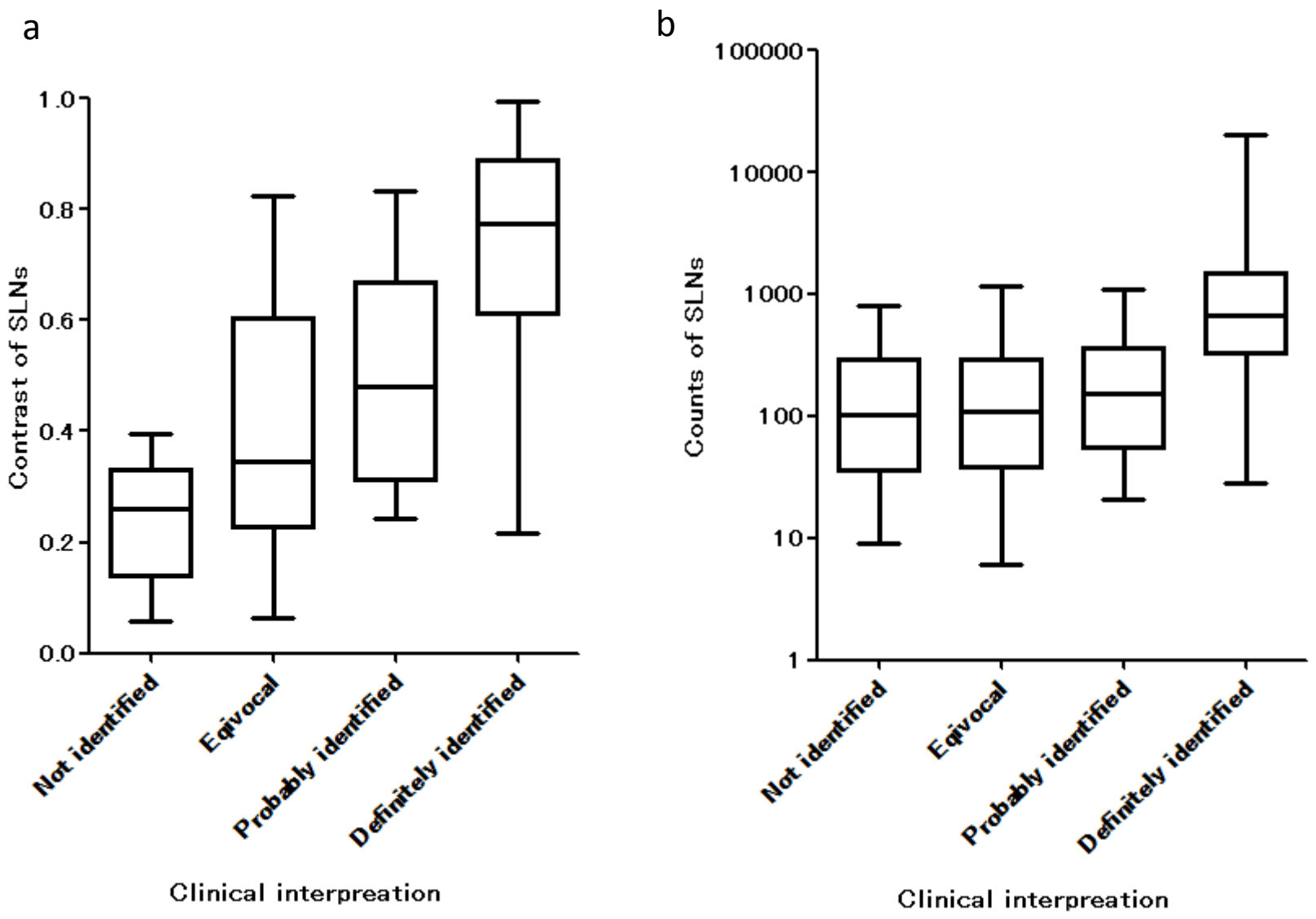
a
1.0
0.8
0.6
0.4
0.2
0.0
Contrast of SLNs
Not identified
Eqivocal
Probably identified
Definitely identified
Clinical interpreation
b
100000
10000
1000
100
10
1
Counts of SLNs
Not identified
Eqivocal
Probably identified
Definitely identified
Clinical interpreation

Fig.8